Breakup-fusion analyses of single-nucleon stripping to bound and unbound orbits

T. Udagawa, Y. J. Lee, and T. Tamura*

Department of Physics, University of Texas, Austin, Texas 78712

(Received 22 July 1987)

A method is presented that is capable of describing on one footing stripping-type reactions, in which the stripped particles are left in either bound or unbound states. The approach is to use the breakup-fusion description even when the stripped particles are bound. Successful applications are presented of this method to a few realistic cases, in which the spin-orbit potential for the stripped particle is taken into account.

I. INTRODUCTION

The stripping-type reaction $A(a,b)B$, in which $a = b + x$ and the particle b is observed, has customarily been treated differently according to the energy E_x of the stripped particle x. Namely, it is treated as the usual stripping reaction if $E_x < 0$, but as a breakup reaction if $E_x > 0$. It is well known that the former (which we shall henceforth simply call the stripping reaction) can be treated very well in terms of the distorted-wave Born approximation (DWBA).[1]

The simplest mode of the breakup-type reactions is elastic breakup (EB) in which both b and x are emitted, leaving the target A in its ground state. However, the contribution from this EB mode to the total b-singles cross section is small in general,[2-5] the dominant contribution coming from the so-called breakup-fusion (BF) reaction[3-5] (or the inelastic-breakup reaction as it is called in Ref. 2). In the BF reaction x is fused with A and only b is emitted. Baur *et al.*[2] analyzed a number of deuteron induced BF reactions, while we ourselves concentrated[3,4] on h and α induced reactions. The formalism on which our calculations were based can be found in Ref. 5. Reference 4 gives further details of numerical calculations along with some numerical results.

Since x is captured during the BF reaction as it is in the stripping reaction, these two reactions are very similar. In fact, the only difference is that in the former the energy E_b of the emitted particle b is such that the corresponding E_x is positive, while in the latter E_x is negative. This strong similarity between these two reactions then suggests that there must be a way to describe them on the same footing, and to show that this is, in fact, the case, is the purpose of this paper. More precisely, we shall show that the BF formalism which has been used exclusively for $E_b \leq E_b^0$ ($E_x \geq 0$) can be used as it stands also for $E_b > E_b^0$ ($E_x < 0$), where E_b^0 is the value of E_b corresponding to $E_x = 0$. A preliminary account of the content of this paper has been reported in Ref. 6.

In the BF method, the relative motion between x and A is described in terms of an optical potential, a concept which is rather clear if $E_x > 0$. The use of a BF method for $E_x < 0$ then requires us to extend the use of an optical potential to negative energy particles. Such an extended use of the optical model has, however, been made by several authors in the past,[7,8] and we shall take advantage of what has been worked out by these authors. As shown in Refs. 7 and 8, the use of a (complex) optical potential gives rise to the spreading of the single-particle strengths. The use of the BF method in the $E_x < 0$ case then gives rise to finite widths of peak cross sections.

In Ref. 6, we analyzed the data of the $^{27}\text{Al}(d,p)$ reaction with $E_d = 25.5$ MeV,[9] and showed that the extended use of the BF method did work nicely. Nevertheless, the work of Ref. 6 was done by assuming that the optical potential for x had no spin-orbit term and, in this work, we want to remove this unsatisfactory feature. It will be seen that once the spin-orbit interaction is explicitly used the extended use of the BF method for $E_x < 0$ begins to provide a powerful spectroscopic tool.

In addition to reanalyzing the $^{27}\text{Al}(d,p)$ reaction data,[9] we shall analyze other data as well in this paper. They are the $^{62}\text{Ni}(d,p)$ reaction with $E_d = 15$ (Refs. 10 and 11) and with 25.5 MeV,[9] and the $^{144}\text{Sm}(\alpha,t)$ reaction with $F_\alpha = 80$ MeV.[12] Among these examples we have picked up, the data of the last, i.e., of the $^{144}\text{Sm}(\alpha,t)$ reaction, has a characteristic feature in that a couple of bumps are observed in the triton spectrum in the region in which E_x, i.e., the energy of the stripped proton, is positive, rather than negative as in other examples. The authors of Ref. 12 performed a spectroscopic analysis for this bumpy spectrum by extending the use of the standard DWBA method (for the $E_x < 0$ region) to the $E_x > 0$ region. With our approach, however, this is the region in which our BF formalism[5] can be applied as it stands, and it will be seen that our straightforward calculation fits the bump spectrum quite well. By combining this with results obtained by analyzing the above (d,p) data, in which bumps appear in the $E_x < 0$ region, one indeed sees that our method works consistently for both $E_x > 0$ and $E_x < 0$ regions.

In Sec. II A, we summarize the BF formulas that are to be used for the present calculations, while in Sec. II B we present a formalism through which the relation between the present calculation and the usual DWBA stripping calculation can be clarified. Analyses of actual data are presented in Sec. III, and the paper is summarized in Sec. IV.

II. FORMULATION OF BREAK-FUSION CALCULATIONS

A. Cross-section formulas

The breakup-fusion reaction may be written symbolically as

$$a + A \rightarrow b + x + A \rightarrow b + B \ . \tag{1}$$

In Eq. (1), the first step (indicated by the first arrow) denotes the breakup of a into $b + x$, while the second step stands for the subsequent fusion (or capture) of x into the target A to form the residual nucleus B. We assume that the particles (b, x, and A) produced in the first breakup step are all in their ground states. This means that the first step is assumed to be what is called the elastic breakup. In the following, we intend to calculate the b-singles cross section in the reaction in (1).

Let us denote the excitation energy of the residual nucleus B by E_{ex}. If the energy carried by the particle i ($i = a$, b, and x) is denoted by E_i E_{ex} is expressed as

$$E_{ex} = E_x + Q_3 - Q_g = E_a - E_b - Q_g \ . \tag{2}$$

Here Q_g and Q_3 are the Q values, respectively, of the stripping reaction $A(a,b)B$ and of the three-body breakup.

We shall call the systems consisting of $a + A$, $b + B$, and $x + A$ the a,b and x channels, respectively. The distorted waves $\chi_i^{(\pm)}$ (with $i = a$, b, and x) in these channels, are given as solutions of the optical-model equation

$$(E_i - T_i - U_i)\chi_i^{(\pm)} = 0 \ . \tag{3}$$

Here T_i and U_i are, respectively, the kinetic energy operator and the optical-model potential.

In our formulation of the BF reaction given so far,[5] we have neglected the spin-orbit interactions in all the U_i. As remarked in the Introduction, we take into account in this paper the spin-orbit interaction $V_{x,so}$ in U_x. However, we still neglect the spin-orbit interactions in U_a and U_b.

The reformulation of the BF calculations[5] required by the introduction of $V_{x,so}$ is straightforward. Thus, we shall just give formulas that are to be used for the calculation presented below.

The double-differential BF cross section is given as

$$\frac{d^2\sigma^{BF}}{dE_b d\Omega_b} = \sum_{l_x j_x} \frac{d^2\sigma^{BF}_{l_x j_x}}{dE_b d\Omega_b} \ , \tag{4}$$

where

$$\frac{d^2\sigma^{BF}_{l_x j_x}}{dE_b d\Omega_b} = (2\pi/\hbar v_a) \frac{2j_x + 1}{(2s_x + 1)(2l_x + 1)} |C^{(2)}_{bx,a}|^2 \rho(E_b)$$

$$\times \sum_{m_x} [\langle u_{l_x j_m m_x} | W_x | u_{l_x j_x m_x} \rangle / \pi] \tag{5}$$

is the partial cross section. In (4) and (5), l_x and j_x are, respectively the orbital and total angular momenta of x. [If we set $j_x = l_x$, and hence suppress j_x entirely from (4) and (5), these equations reduce to those in Ref. 5.] $C^{(2)}_{bx,a}$

in (5) is the spectroscopic amplitude,[13] while $\rho(E_b)$ is the phase-space volume of the emitted particle b given as

$$\rho(E_b) = (\hbar^2 k_b) / [(2\pi)^3 \mu_b] \ . \tag{6}$$

In (6), k_b and μ_b are the wave number and the reduced mass of b, respectively.

Further in (5), v_a is the incident velocity, while W_x is the negative of the imaginary part of $U_x (= -V_x - iW_x)$. The function $u_{l_x j_x m_x}(r)$ is the x-channel partial wave function that describes the motion of x with respect to A. It satisfies the inhomogeneous equation given as

$$(h_x - E_x)u_{l_x j_x m_x}(r) = \rho_{l_x j_x m_x}(r) \ , \tag{7}$$

$$h_x = -\frac{\hbar^2}{2\mu_x} \left[\frac{d^2}{dr^2} - \frac{l_x(l_x + 1)}{r^2} \right] + U_{x;l_x j_x} \ . \tag{8}$$

The $\rho_{l_x j_x m_s}(r)$ on the rhs of Eq. (7) is the source function (for creating the particle x) and is defined as

$$\rho_{l_x j_x m_x}(r) = r \langle \chi_b^{(-)} i^{l_x} Y_{l_x m_x} | V_{a,l_x j_x} | \chi_a^{(\pm)} \varphi_{bx} \rangle \ . \tag{9}$$

Here $Y_{l_x m_x}$ is the spherical harmonics, while φ_{bx} is the wave function for the relative motion between b and x in a. Furthermore, $V_{a;l_x j_x}$ is defined by

$$V_{a;l_x j_x} = U_{x,l_x j_x} + U_b - U_a \ , \tag{10}$$

where $U_{x,l_x j_x}$, which appeared also in (8), is defined by

$$U_{x,l_x j_x} = \langle \phi_{l_x s_x j_x m_x} | U_x | \phi_{l_x s_x j_x m_x} \rangle \ , \tag{11a}$$

$$\phi_{l_x s_x j_x m_x} = \sum_{m_l m_s} \langle l_x m_l s_x m_s | j_x m_x \rangle i^{l_x} Y_{l_x m_l} \varphi_x \ . \tag{11b}$$

Here φ_x is the spin-isospin wave function for x.

The formulas given above can be used for both $E_x > 0$ and $E_x < 0$ cases. However, in solving Eq. (7) to obtain $u_{l_x j_m m_x}$, the outgoing boundary condition is to be imposed upon $u_{l_x j_x m_x}$ when $E_x > 0$. On the other hand, the exponential-decay boundary condition is to be imposed when $E_x < 0$.

For the $E_x < 0$ case, the BF cross section given by (4) is by itself the b-singles cross section. For the $E_x > 0$ case, however, the cross section for the EB reaction must be added to the BF cross section. This EB cross section can be given, by using notation already explained, as

$$\frac{d^2\sigma^{EB}}{dE_b d\Omega_b} = \sum_{l_x j_x} \frac{d^2\sigma^{EB}_{l_x j_x}}{dE_b d\Omega_b} \ , \tag{12}$$

$$\frac{d^2\sigma^{EB}_{l_x j_x}}{dE_b d\Omega_b} = \frac{2\pi}{\hbar v_a} \rho(E_b) \frac{2j_x + 1}{(2s_x + 1)(2l_x + 1)} |C^{(2)}_{bx,a}|^2$$

$$\times \sum_{m_x} \left| \frac{4\pi}{k_b} \int \chi_{l_x j_x}^{(-)}(r) \rho_{l_x j_x m_x}(r) dr \right|^2 \ . \tag{13}$$

B. Remarks about the use of the BF formula for $E_x < 0$

Actual numerical calculations to be given in Sec. III are done for both $E_X > 0$ and $E_x < 0$ regions by using the formulas already given in Sec. II A. Therefore, for the purpose of the calculations, it is unnecessary to continue the discussion of the formalism any further. We, nevertheless, want to give a qualitative argument about the use of the BF formula for the $E_x < 0$ case. We do this because such a use is new in this paper, while the use of the BF formula for the $E_x > 0$ case is now rather well understood.[3-5]

In the following, we in particular want to show that the BF cross section obtained for the $E_x < 0$ case is nothing but an energy average of the usual DWBA cross sections of the stripping reactions. To do this, we make a simplifying assumption that W_x is a constant, i.e., that it is simply given as

$$W_x = -\Gamma/2 . \tag{14}$$

Let us denote by h_x^0 the optical-model Hamiltonian h_x [defined in (8)], when W_x is set to zero in the latter. We then consider a set of (real) eigensolutions $\{\psi_i\}$ of this new Hamiltonian h_x^0:

$$(h_x^0 - E_i)\psi_i = 0 . \tag{15}$$

Clearly h_x^0 can be regarded as the radial single-particle shell-model Hamiltonian, and ψ_i and E_i as the corresponding single-particle wave function and energy, respectively.

Under the assumption that W_x is a constant, ψ_i also satisfies

$$(h_x - \tilde{E}_i)\psi_i = 0 , \tag{16a}$$

with

$$\tilde{E}_i = E_i - i\Gamma/2 . \tag{16b}$$

Namely, ψ_i is an eigenfunction of the complex Hamiltonian h_x with the complex eigenvalue $\tilde{E}_i$. The imaginary part Γ then describes the spreading (decaying) width of the eigenstate i.[8] It is positive, because of the absorptive nature of W_x. [In the time-dependent description, the single-particle wave function in the potential with such an imaginary part as given by (14) is a decaying state. The reader may refer to Ref. 8 for more detail on this point.]

In terms of $\{\psi_i\}$, one can expand $u_{l_x j_x m_x}$ as

$$u_{l_x j_x m_x} = \sum_i \frac{1}{E_x - E_i + i\Gamma/2} |\psi_i\rangle\langle\psi_i|\rho_{l_x j_x m_x}\rangle . \tag{17}$$

Note that the sum over i in the Eq. (17) is over the complete set of states i, which includes not only the discrete (bound) states, but also the continuum states with $E_x > 0$. Therefore, $u_{l_x j_x m_x}$ given by (17) includes continuum effects.

By using (17), the matrix element in (5), is written as

$$\langle u_{l_x j_x m_x}|W_x|u_{l_x j_x m_x}\rangle$$

$$= \sum_i \frac{\langle\psi_i|W_x|\psi_i\rangle}{(E - E_i)^2 + \Gamma^2/4}|\langle\psi_i|\rho_{l_x j_x m_x}\rangle|^2 . \tag{18}$$

Inserting (18) into (5), we finally obtain

$$\frac{d^2\sigma_{l_x j_x}^{\text{BF}}}{dE_b d\Omega_b} = \sum_i S_i \frac{d\sigma_{l_x j_x}}{d\Omega_b} , \tag{19a}$$

where

$$\frac{d\sigma_{l_x j_x}}{d\Omega_b} = \frac{2\pi}{\hbar v_a}\rho(E_b)$$

$$\times \frac{2j_x + 1}{(2s_x + 1)(2l_x + 1)}|C_{bx,a}^{(2)}|^2|\langle\psi_i|\rho\rangle|^2 , \tag{19b}$$

$$S_i = \frac{\Gamma}{2\pi}\frac{1}{(E - E_i)^2 + \Gamma^2/4} . \tag{19c}$$

The *single*-differential cross section given by (19b) is nothing but the usual DWBA cross section of the stripping reaction, in which x is captured into a single-particle state i. Also, S_i given by (19c) is the single-particle strength function.[8] It is thus seen that the *double*-differential cross section of (19a) is, in fact, an energy average of the DWBA cross sections of (19b) that have S_i as their weight functions. In the limit of $W \to 0$, S_i reduces to a delta function $\delta(E - E_i)$. Equation (19a) then reduces to a sum of the usual DWBA cross sections that are spiked at discrete energies. [We note that the width Γ of the above energy average originates from W_x in the propagator in

$$u_{l_x j_x m_x}(r) = \rho_{l_x j_x m_x}(r)/(h_x - E_x) ,$$

which is obtained by solving Eq. (7). This in turn clarifies the physical significance of W_x present in the propagator.]

The formulas given so far in this subsection were derived by assuming a constant W_x. It was also assumed implicitly that V_x was energy independent, because otherwise the formalism would have been much more complicated. In any case, what we have shown is that the result summarized by (19) (which may simply be written down intuitively without derivation) can be obtained only under these rather restrictive assumptions.

In using the formulas developed in Sec. II A, however, it is unnecessary to make any of these assumptions. Both V_x and W_x may depend on E_x and r_x. Thus, the calculations done by using the BF formula of Sec. II A do describe the reaction which is more sophisticated than what is described by (19). Nevertheless, the fact that such calculations result in energy-averaged cross sections, as demonstrated by (19), may remain to be true to a large extent.

We may finally remark on the validity of the use of our BF formula at a very small excitation energy (E_{ex}) region. This is the region, where we observe discrete state transitions. There the measured cross sections are normally analyzed in terms of the standard DWBA method,[1] deducing the spectroscopic factors S for the final states. The values of the S factors thus determined often fluctuate strongly from a state to another. As remarked above, however, the BF approach describes only the energy averaged behavior of the S factors. Therefore, it does not

make much sense to apply such a description to a very small E_{ex} region, where the level density is very low and the S factor fluctuates strongly. Thus, we shall not attempt in this paper to fit data at very low E_{ex}.

Even in the excitation region where states are still discrete, we may still apply the present method, if the density of the states is high. Some of the experimental data we have picked up to analyze have been given in the form of discrete state cross sections, and we shall fit these data after averaging these cross sections over appropriate energy bins.

III. APPLICATIONS

We shall now report on numerical calculations. Below we consider the partial BF and EB cross sections, given by Eqs. (5) and (13), respectively, and also of their sum, which we denote simply by $\sigma_{l_x j_x}^{th}$:

$$\sigma_{l_x j_x}^{th} = \frac{d^2 \sigma_{l_x j_x}^{EB}}{dE_b d\Omega_b} + \frac{d^2 \sigma_{l_x j_x}^{BF}}{dE_b d\Omega_b} \ . \tag{20}$$

(As noted above the EB cross section is zero for $E_x < 0$.) We also consider the sum over partial cross sections, and denote it by σ^{th}. Thus,

$$\sigma^{th} = \sum_{l_x j_x} \sigma_{l_x j_x}^{th} \ . \tag{21}$$

We performed BF calculations for four reactions. They are the ^{27}Al$(d,p)^{28}$Al reaction with $E_p = 25.5$ MeV,[9] the ^{62}Ni$(d,p)^{63}$Ni reaction with $E_d = 15$ MeV (Refs. 10 and 11) and with $E_d = 25.5$ MeV,[9] and finally the ^{144}Sm$(\alpha,t)^{145}$Eu reaction with $E_\alpha = 80$ MeV.[12] All the

calculations were carried out by taking into account finite-range effects exactly. Since our cross section formulas use the prior-form interaction $V_{a,l_x j_x}$ [see Eq. (10)], it is indispensable to carry out finite-range calculations exactly.[13] The details of how we perform such calculations were given in Ref. 4.

The parameters involved in the present calculations are mostly those of the optical potentials, and the values that are used are summarized in Table I. As seen, those for the (d,p) reactions were taken from Perey and Perey,[14] while those for (α,t) reactions were taken from Ref. 12. On the other hand, the parameters used for the potentials for x are those that were obtained by slightly modifying those found in the literature, so that the energies of the single-particle states become consistent with experiment. (This is essentially the same as what is done in the well-known separation energy method.[1]) As for W_x for $E_x < 0$, there is essentially no information available in the literature. We fixed its value so that the widths of the single-particle states are appropriately reproduced in the $E_x < 0$ region, and then increased linearly in the $E_x > 0$ region untile E_x becomes sufficiently high so that W_x is known from optical-model analysis.

In fixing the wave function φ_{bx}, we used the Hulthen-type wave function when the projectile was d, while we generated φ_{bx} for the t-p system [needed in describing the (α,t) reaction] by assuming a Woods-Saxon potential between p and t with $V_0 = 66.2$ MeV, $a_0 = 0.67$ fm, and $r_0 = 1.2$ fm. This potential reproduces the correct separation energy of 19.8 MeV. It also gives the zero-range constant parameter of $D_0 = 309$ MeV fm$^{3/2}$, which is very close to that used in the usual zero-range calculations.[12]

TABLE I. Optical-model potential parameters.

Reaction	E_a (MeV)	Particle	V_R (MeV)	r_R (fm)	a_R (fm)	W (MeV)	r_I (fm)	a_I (fm)	W_D (MeV)	r_D (fm)	a_D (fm)
^{27}Al(d,p)	25.5	d	103.60	1.02	0.85				11.82	1.413	0.695
		p	51.80	1.29	0.48	8.6	1.29	0.48			
		n	58.30	1.25	0.65				2–9[a]	1.25	0.65
^{62}Ni(d,p)	15.0	d	91.84	1.15	0.81				18.00	1.34	0.68
		p	52.30	1.25	0.65				14.60	1.25	0.47
		n	55.00	1.25	0.65				2–9[b]	1.25	0.65
	25.5	d	89.54	1.15	0.81				20.52	1.34	0.68
		p	50.92	1.21	0.75				13.08	1.32	0.46
		n	55.00	1.25	0.65				2–9[b]	1.25	0.65
^{144}Sm(α,t)	80.0	α	158.40	1.32	0.62	30.02	1.35	0.85			
		t	125.40	1.18	0.86	17.20	1.55	0.77			
		p	59.40	1.25	0.65	1–3[c]	1.25	0.65			

Spin-orbit parameters

			V_{so}	r_{so}	a_{so}
^{27}Al(d,p)		n	6.00	1.01	0.75
^{62}Ni(d,p)		n	6.20	1.01	0.75
^{144}Sm(a,t)		p	6.40	1.10	0.65

[a]$W_D = 2.0$, 9.0, for $E_n < 0$, > 6.0 MeV, and $W_D = 2.5 + E_n$ for $0 \le E_n \le 6$ MeV.
[b]$W_D = 2.0$, 5.5, and 9.0 MeV for $E_n < 0.3$, $= 0.3$ and > 0.3 MeV.
[c]$W = 1.0$, 3.0 for $E_p \le 2.7$, > 2.7 MeV.

A. The ^{27}Al$(d,p)^{28}$Al reaction with $E_d = 25.5$ MeV

We first consider the ^{27}Al$(d,p)^{28}$Al reaction with $E_d = 25.5$ MeV (Ref. 9) which is the reaction also considered in Ref. 6. In this reaction, we have $a = d$, $b = p$, and $x = n$, and the energetics are given by $E_p + E_n = 21.5$ MeV (in c.m.). The spectrum given in Ref. 9 shows a bump at $E_p = 24.5$ MeV $(E_n = -3$ MeV) (see Fig. 1), and in Ref. 6 we ascribed it to a resonance due to the $f_{7/2}$ single-particle state.[15] In Ref. 6, however, we neglected the spin-orbit interaction (for $x = n$), and were forced to subtract rather artificially the $f_{5/2}$ strength in fitting the calculated spectrum to the data. We repeat here the same calculation, but including the spin-orbit interaction this time.

The result of the calculation is presented in Fig. 1 (solid line) and is compared with experiment. In presenting the theoretical cross section σ^{th}, an overall normalization constant $N = 0.9$ which is very close to 1 was used. Also, in obtaining σ^{th}, we used $W_n = 2$ MeV for $E_p > 21.5$ MeV (i.e., for $E_n < 0$). The value of W_n was then increased linearly up to 9 MeV as E_p was decreased from 21 to 16 MeV. For $E_p < 16$ MeV $(E_n > 5.5$ MeV), W_n was fixed to 9 MeV, which is the value determined from the neutron elastic scattering data.[14]

As seen in Fig. 1, σ^{th} fits the experimental cross section σ^{exp} very well in both $E_x > 0$ and $E_x < 0$ regions, except at two extremes of very high and low E_p. The highest E_p region is not where we intend to apply the present method; see the remark at the end of Sec. II B. The
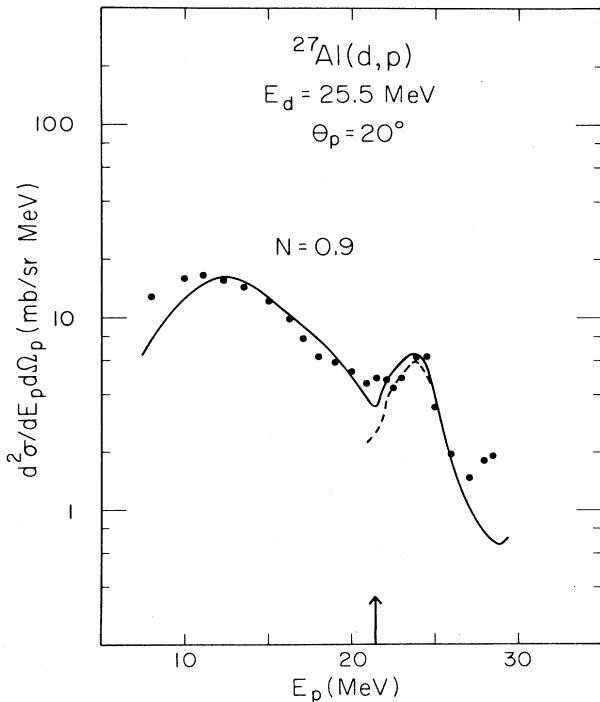

FIG. 1. Experimental and calculated energy spectra for the ^{27}Al(d,p) reaction at $E_d = 25.5$ MeV and $\vartheta_p = 20°$. The data were taken from Ref. 9. The solid line includes all the contributions, while the dashed line includes only $f_{7/2}$, $p_{3/2}$, and $p_{1/2}$ contributions. The arrow shows the energy where $E_n = 0$.

discrepancy seen in the lowest E_p region may simply be attributed to higher-order processes (including compound nuclear processes) that have not been taken into account in the present calculation.

It is remarkable that the calculations reproduce the resonance observed at $E_p \simeq 24.5$ MeV very well. As remarked above, this resonance was attributed in Ref. 6 to that of the $f_{7/2}$ single-particle state. According to the present calculation, however, the peak actually consists of many components, being dominated by the $f_{7/2}$ (at $E_p \simeq 24.3$), $p_{3/2}$ (at $E_p \simeq 23.3$ MeV), and $p_{1/2}$ (at $E_p \simeq 22$ MeV) components. The dashed line shown in Fig. 1 represents the sum of the $f_{7/2}$, $p_{3/2}$, and $p_{1/2}$ contributions and it is indeed seen that the observed peak cross section is dominated by these three. It is also remarkable that now we do not need to artificially suppress the $f_{5/2}$ contribution. The $f_{5/2}$ strength has been shifted to higher energies due to the presence of the spin-orbit interaction. In this sense, the present calculation is much more straightforward than that in Ref. 6.

B. The ^{62}Ni$(d,p)^{63}$Ni reaction with $E_d = 15$ and 25.5 MeV

As the next example, we consider the ^{62}Ni$(d,p)^{63}$Ni reaction with the incident energy $E_d = 15$ (Refs. 10 and 11) and 25.5 MeV.[9] We have again $a = d$, $b = p$, and $x = n$, and in the c.m. they are $E_p + E_n = 12.3$ and 22.5 MeV, respectively. For the $E_d = 15$ MeV case, data were taken by Fulmer and McCarthy[10] up to $E_{\text{ex}} = 6.5$ MeV with very high resolution. Thus, cross sections resulting in about 40 individual final states were obtained and for all these cross sections the DWBA analyses were done to extract the spectroscopic factors and the l_n values. The results of these analyses and also the measured peak cross sections were tabulated in Table II of Ref. 10.

For the $E_d = 15$ MeV case, data were also taken of the p-singles cross sections[9] over a wide range of E_p $(E_p = 5$-19 MeV) including the breakup peak region. Here we consider both sets of data. For the $E_d = 25.5$ MeV case, similar data are available[9] and we also analyze them.

1. $E_d = 15$ MeV case

In Figs. 2(a)–(c), using 1-MeV-step histograms we present the measured peak cross sections separately for (a) $l_n = 0$, (b) $l_n = 2$, and (c) $l_n = 4$ transitions. The peak angles of the $l_n = 0$, 2, and 4 cross sections are $\vartheta = 9°$, 23°, and 37°, respectively, and the spectra shown in Figs. 2(a)–(c) are those at these angles.

The solid lines shown in Fig. 2 are for the calculated partial cross sections $\sigma^{\text{th}}_{l_n} = \sigma^{\text{th}}_{j_{n>}} + \sigma^{\text{th}}_{j_{n<}}$, where $\sigma^{\text{th}}_{j_{n>}}$ and $\sigma^{\text{th}}_{j_{n<}}$ are the cross sections with $j_{n>} = l_n + \frac{1}{2}$ and $j_{n<} = l_n - \frac{1}{2}$, respectively. The $\sigma^{\text{th}}_{j_{n>}}$ and $\sigma^{\text{th}}_{j_{n<}}$ are also presented separately in Fig. 2 by dashed lines. In calculating these cross sections, the strength of W_n was fixed at 2 MeV.

As seen in Fig. 2(b), the experimental $l_n = 2$ cross sections are rather well reproduced by our calculations. It is also seen that our calculations explain the observed cross
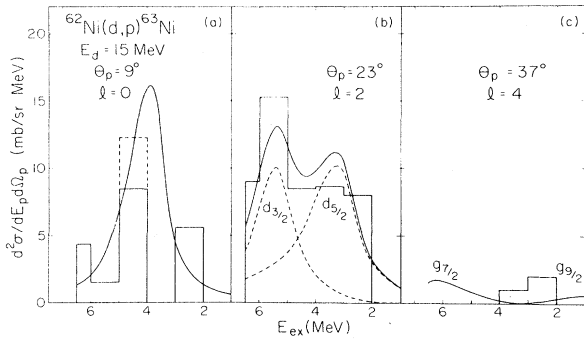
FIG. 2. Experimental and calculated partial cross sections for the ^{62}Ni$(d,p)^{63}$Ni reaction at $E_d = 15$ MeV, and (a) at $\vartheta_p = 9°$ for $l_n = 0$, (b) at $\vartheta_p = 23°$ for $l_n = 2$, and (c) at $\vartheta_p = 37°$ for $l_n = 4$. The experimental data are given in the form of a histogram with a 1 MeV bin in the range of 2–6.5 MeV of the excitation energy. The solid curves represent the sum of the $j_<$ and $j_>$ cross sections where $j_< = l_n - \frac{1}{2}$ and $j_> = l_n + 1$. The dashed curves are for partial cross sections with definite j values. The experimental data were taken from Ref. 10. (See text for the dotted histogram shown for $l_n = 0$ case.)

section in the $E_{ex} = 2.0$–4.5 MeV region as essentially due to the $d_{5/2}$ contributions, and that in the $E_{ex} > 4.5$ MeV region as due to the $d_{3/2}$ contributions. It is worthwhile to remark that the $l_n = 2$ states for $E_{ex} \leq 4.4$ MeV were identified as $d_{5/2}$ states, from an experiment which measured asymmetry.[16] The result of the present analysis is in line with this experimental information.

Previously the position of the $d_{3/2}$ states was not known. The good fit of the calculated $d_{3/2}$ cross section to the data for $E_{ex} = 4.5$–6.5 MeV will permit us to conclude that the $l_n = 2$ strength in this region is, in fact, due to the $d_{3/2}$ state. The centroid of the $d_{3/2}$ state is determined as 5.5 MeV.

It is notable that the width $\Gamma_{5/2}$ ($\simeq 2.2$ MeV) of $\sigma_{5/2}^{th}$ turned out to be larger than the width $\Gamma_{3/2}$ ($\simeq 1.7$ MeV) of $\sigma_{3/2}^{th}$. As seen in Fig. 2(b), to have this inequality $\Gamma_{5/2} > \Gamma_{3/2}$ was vital in obtaining the good fit to the data there. We want to emphasize that the curve in Fig. 2(b) was obtained as a result of the straightforward BF calculations that used formulas of Sec. II A, and that the $\Gamma_{5/2}$ and $\Gamma_{3/2}$ values quoted above were simply read off from this curve.

Let us now tun to the $l_n = 0$ and 4 cross sections. The fit of the calculated cross section to the experimental data is fairly good, but is not as good as it was with the $l_n = 2$ case. This may have been caused partially by a less accurate determination of the experimental strength for these cross sections. In any case the $l_n = 4$ transitions are very weak (for the incident energy considered here). It also appears that there is an experimetnal difficulty in separating the $l_n = 0$ transitions from the $l_n = 2$ transitions. For instance, the transition to the ~ 4.1 MeV state was assigned as that of $l_n = 2$ in Ref. 10, but as that of $l_n = 0$ in Ref. 17. The dotted line shown in Fig. 2(a) is the experimental $l_n = 0$ cross section obtained when the above transition is assigned as that of $l_n = 0$. Our $l_n = 0$ cross sec-

tion agrees rather well with these newly constructed data.[17]

In Fig. 3, we present σ^{th} at $\vartheta_p = 23°$ and compare it with σ^{exp} of Ref. 11 that ranges from $E_n < 0$ to $E_n > 0$ regions. In obtaining the σth, we used $W_n = 2$ MeV for $E_p > 13$ MeV ($E_n < 0$), but increased W_n linearly from 2 to 9 MeV as E_p decreased from 13 to 11 MeV. For $E_p < 11$ MeV, W_n was fixed to 9 MeV, which is the value determined from the analysis of the elastic scattering data.[14] The original data in Ref. 11 were taken with 0.5 MeV bins. In plotting the data in Fig. 3, however, we increased the size of the bin to 1 MeV. We simply averaged the cross sections of the successive bins in doing this.

The fit of σth to σ^{exp} is good. It is remarkable that the broad peak observed at $E_p \simeq 13.7$ MeV ($E_{ex} \simeq 5.3$ MeV) is well reproduced in the calculation. This peak is due to the $d_{3/2}$ state discussed above. On the other hand, we see a discrepancy for $E_p \simeq 16$ MeV ($E_{ex} \simeq 3$ MeV) where we achieved good fit to data in Fig. 2(b). This discrepancy has been caused by an unfortunate inconsistency between the data of Refs. 10 and 11. In Fig. 3 we see a dip at $E_p = 16$ MeV which corresponds to $E_{ex} = 3.0$ MeV. In Fig. 2(b), however, we see a $d_{5/2}$ peak there.

2. $E_d = 25.5$ MeV case

In Fig. 4 a similar analysis as done in Fig. 3 for the $E_d = 15$ MeV case is extended to the $E_d = 25.5$ MeV case. We used the same W_x (as a function of E_{ex}) as used for Fig. 3. As seen, the fit of σth to σ^{exp} is very good. Note that in the calculated spectrum for $E_d = 15.0$ MeV (see Fig. 3), we observed a dip at $E_p = 15$ MeV that corresponds to $E_{ex} = 4.5$ MeV. Such a dip, however, does not
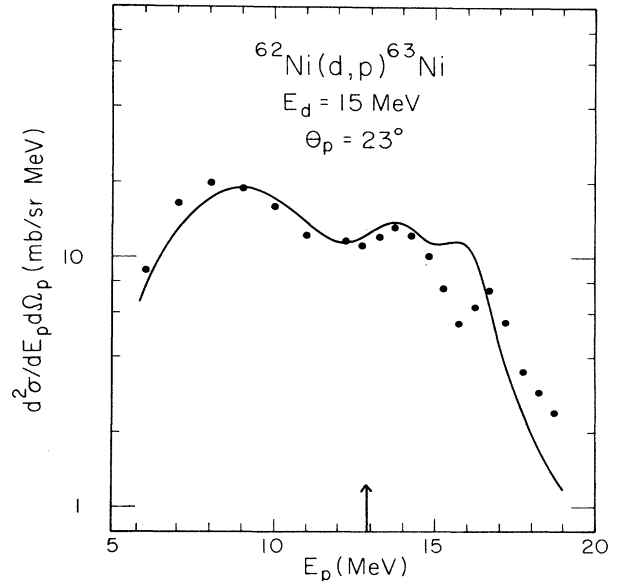

FIG. 3. Experimental and calculated energy spectrum for the ^{62}Ni$(d,p)^{63}$Ni reaction at $E_d = 15$ MeV and $\vartheta_p = 23°$. The data are taken from Ref. 11. The arrow shows the energy where $E_n = 0$.

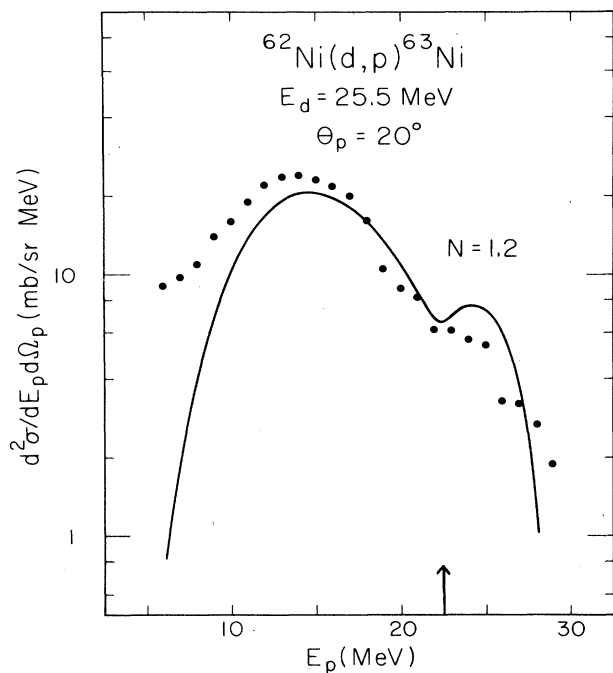FIG. 4. Experimental and calculated energy spectrum for the ^{62}Ni$(d,p)^{63}$Ni reaction at $E_d = 25.5$ MeV and $\vartheta_p = 20°$. The data are taken from Ref. 9. The arrow shows the energy where $E_n = 0$.

FIG. 5. Experimental and calculated energy spectra for the ^{144}Sm$(\alpha, t)^{145}$Eu reaction at $E_\alpha = 80$ MeV and $\vartheta_t = 4°$. The solid line represents the total theoretical cross section. The dotted lines represent the $f_{7/2}$, $h_{9/2}$, and $i_{13/2}$ partial cross sections, while the dot-dashed line represents their sum. The data were taken from Ref. 12. The arrow shows the energy where $E_p = 0$.

appear at $E_d = 25.5$ MeV. This resulted because the relative importance of the $l = 4$ cross section has increased.

C. The ^{144}Sm$(\alpha, t)^{145}$Eu reaction with $E_\alpha = 80$ MeV

As a final example, we take the ^{144}Sm$(\alpha, t)^{145}$Eu reaction with $E_\alpha = 80$ MeV, the data being provided by Gales et al.[12] In the case of this reaction, we have $a = \alpha$, $b = t$, and $x = p$, and in the c.m., $E_t + E_n = 58.0$ MeV. In the measured triton spectra, two broad bumps were observed in the continuum $(E_x = E_p > 0)$ region at $E_{ex} = 5.9$ and 7.6 MeV. $(E_{ex} = 3.4$ MeV corresponds to $E_p = 0$.) By first subtracting the background components, Gales, et al.[12] extracted the resonance cross sections, and determined the widths of the resonances at $E_{ex} = 5.9$ and 7.6 MeV as 1.2 and 4.0 MeV, respectively. The DWBA analysis of the cross sections was also done[12] by using Gamov functions[18] as form factors for the unbound proton. The result of the analysis showed that the peaks at 5.9 and 7.6 MeV were those of the $h_{9/2}$ and $i_{13/2}$ single-particle states, respectively.

In Fig. 5, we present our σ^{th} calculated at $\vartheta = 4°$ (solid line) and compare it with σ^{exp}.[12] There, we also present by dotted lines the $f_{5/2}$, $h_{9/2}$, and $i_{13/2}$ partial cross sections. In obtaining these cross sections, we used $W_p = 1$ MeV for $E_{ex} < 6.0$ MeV $(E_p < 2.7$ MeV), and $W_p = 3$ MeV for $E_{ex} > 6.0$ MeV. In plotting the theoretical cross sections, we introduced a normalization factor of $N = 0.8$, which is again sufficiently close to 1. It is remarkable
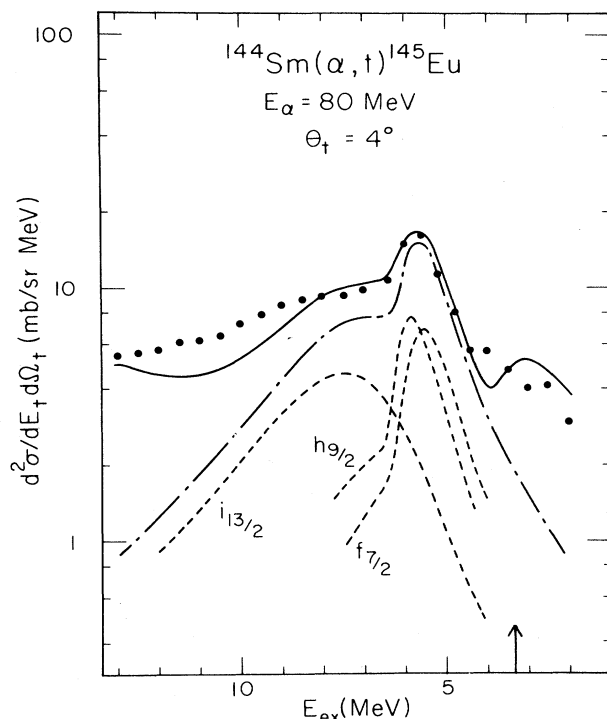
that the observed spectrum, including the bumps are well reproduced by the calculation.

It is seen in Fig. 5, that the observed resonance at $E_{ex} = 5.7$ MeV is explained essentially in terms of the sum of the $h_{9/2}$ and $f_{7/2}$ partial cross sections, both contributing almost equally with about the same positions of the peaks. Note that in Ref. 12, the centroid of the $f_{7/2}$ state was located at $E_x = 4.3$ MeV, which is lower than 5.5 MeV located in the present calculation.

In the analysis of Ref. 12, it was concluded that 43% of the total $f_{7/2}$ strength was in the region of $E_{ex} = 2-9$ MeV, while 75% of the $h_{9/2}$ strength was in the $E_{ex} = 3-12$ MeV region. According to the present calculation shown in Fig. 5, however, their full strengths should be found in these regions.

These different conclusions about the transition strengths were drawn, because there is a difference in handling the background in Ref. 12 and here. In Ref. 12, part of the observed cross section was somewhat arbitrarily assigned as the background (which amounted to about a quarter of the observed cross section at $E_{ex} \simeq 5.7$ MeV). With our calculations, on other hand, no corresponding subtraction was done and the cross section which may be called the background cross section (the sum of the EB plus the BF partial cross sections other

T. UDAGAWA, Y. J. LEE, AND T. TAMURA

than from $f_{5/2}$, $h_{9/2}$, and $i_{13/2}$ states) turns out to be only 5% of the observed cross section (at $E_{ex} \simeq 5.7$ MeV). Note that the calculated EB cross section was found to be extremely small, being less than 1% (at $E_{ex} \simeq 5.7$ MeV) even including the Coulomb breakup. This is due to the effect of Coulomb repulsion upon the emitted protons.

The analysis of Ref. 12 assigned the broad bump observed at $E_{ex} \simeq 7.6$ MeV to the resonance of the $i_{13/2}$ state. The present calculation predicted a broad resonance shaped $i_{13/2}$ cross section, with its peak located at $E_{ex} = 7.5$ MeV, agreeing with the assignment made in Ref. 12. Our calculation predicted the width to be about 4.0 MeV, which again agrees with what was extracted in Ref. 12. In Ref. 12, however, only about 54% of the total $i_{13/2}$ strength was assigned in the $E_{ex} = 2-12$ MeV region, while the present calculation located about 95% of the total strength in this region. The difference again originates from the way the background is handled. The background cross section was found in the present calculations to be 30% of the total σ^{th} at the peak region ($E_{ex} \simeq 7.6$ MeV), while in Ref. 12 50% of the measured cross section was assigned to the background.

In Fig. 6, we present an example of fitting the angular distribution. As seen, the calculated angular distribution (at $E_{ex} = 5.5$ MeV) agrees very well with the data[12]. A

similarly good fit to the observed angular distribution was obtained in Ref. 12.

IV. CONCLUDING REMARKS

The breakup-fusion description was applied to calculate spectra of the $^{27}Al(d,p)$, $^{62}Ni(d,p)$, and $^{144}Sm(\alpha,p)$ reactions leading to both bound ($E_x < 0$) and unbound ($E_x > 0$) regions, where E_x is the energy of the stripped particle [neutron for the (d,p) reaction and proton for the (α,t) reaction]. We showed that the calculated spectra fit the data in both regions very nicely.

It was also demonstrated that our BF method can be used for obtaining information about high-lying single-particle states. In fact, we were able to locate the $f_{7/2}$ state in ^{28}Al, the $d_{3/2}$ state in ^{63}Ni and the $f_{7/2}$, $h_{9/2}$, and i_{13} states in ^{145}Eu. Note that these single-particle states in ^{145}Eu are all in the continuum region.

As we stressed in the Introduction, the application of our BF description has largely been concentrated on h and α induced reactions, and thus the present work is regarded as the first detailed application of our method to the analysis of the (d,p) reactions. In this sense, it is rather pleasing to find that our method works rather well not only for the $E_n < 0$ region (which is new in this paper), but also for the $E_n > 0$ region, where the application of our BF formula[5] is much more straightforward.

Actually there has been a reason why we have been somewhat hesitant in the past in performing a BF analysis of the (d,p) data, the reason being the lack of sufficient knowledge about the neutron potential to be used when E_n was rather close to zero. In the present work, however, it has become possible to perform a consistent analysis of data with $E_n \gtrless 0$. The approach that we took was to perform the analysis of the $E_n < 0$ data first, which permitted us to fix the neutron potential rather severely, because it must let several single-particle states be located at the right energies. We then used the same potential also for the $E_n > 0$ region, and it became possible to perform the BF calculation there with a rather high confidence. The fact that we were able to fit several (d,p) data with normalization factor N very close to unity ($N = 0.8-0.9$) may be regarded as an a posteriori confirmation of the validity of our method to describe the (d,p) reactions in the BF way.

Regarding the $^{144}Sm(\alpha,t)^{145}Eu$ reaction, we have compared our analysis with that in Ref. 12, which utilized the standard DWBA method in the $E_p > 0$ region. In principle, there is nothing wrong in doing this, but it appears that this method encounters in practice a difficulty in handling the weak contributions from nonresonant partial waves. Because of this, the authors of Ref. 12 were forced to make an arbitrary subtraction of the background. With our approach, however, the background-like and the resonancelike partial waves are treated on a completely equal footing, thus leaving essentially no room for ambiguity of the calculations due to subtraction. We thus believe that the spectroscopic information extracted in our way can be taken rather seriously.

The method of using an optical potential to describe bound particles, as in this paper, may be extended to de-
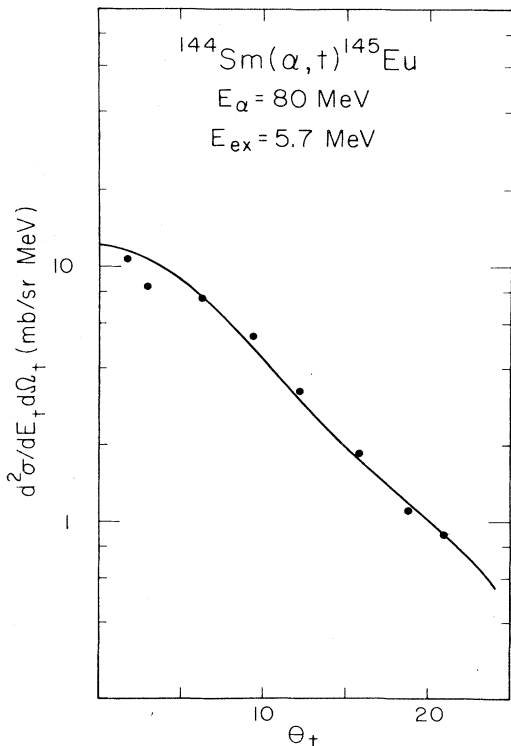

FIG. 6. Experimental and calculated angular distributions for the $^{144}Sm(\alpha,t)^{145}Eu$ reaction at $E_\alpha = 80$ MeV and $E_{ex} = 5.6$ MeV. The experimental data plotted are an average of the cross section over $E_{ex} = 5-6$ MeV. The data were taken from Ref. 12.

scribe other reactions as well. Consider, for instance, an inelastic excitation of a target nucleon from an occupied orbit to an unoccupied orbit. We may describe the final (single-particle) states by means of the optical-model potential. This means that a unified description of inelastic excitations into the bound and unbound orbit is possible. The inelastic excitations into unbound orbits were successfully described as a knockout-fusion process.[19] This process can now be extended to describe inelastic excitations into bound orbits as well.

ACKNOWLEDGMENTS

*Deceased on October 10, 1988.

[1]N. Austern, *Direct Reaction Theories* (Wiley-Interscience, New York, 1970); G. R. Satchler, *Direct Nuclear Reactions* (Oxford University Press, New York, 1983).

[2]G. Baur, F. Rösel, D. Trautman, and R. Shaym, Phys. Rep. **111**, 333 (1983).

[3]T. Udagawa, D. Price, and T. Tamura, Phys. Lett. **118B**, 45 (1982); T. Udagawa, X. H. Li, and T. Tamura, Phys. Lett. **135B**, 333 (1984); *ibid.* **143B**, 15 (1984).

[4]T. Udagawa, H.-X. Li, and T. Udagawa, Phys. Rev. C **37**, 429 (1988).

[5]T. Udagawa and T. Tamura, Phys. Rev. C **24**, 1348 (1981); **33**, 494 (1986).

[6]T. Udagawa, Y. J. Lee, and T. Tamura, Phys. Lett. B **196**, 291 (1987).

[7]D. H. Gross and R. Lipenheide, Nucl. Phys. **A150**, 449 (1970); C. A. Engelbrecht and H. A. Weidenmüller, *ibid.* **A184**, 385 (1972).

[8]C. Mahaux, P. F. Bortignon, R. A. Broglia, and C. H. Dasso, Phys. Rep. **120**, 1 (1985).

[9]J. Pampus *et al.*, Nucl. Phys. **A311**, 141 (1978).

[10]R. H. Fulmer and A. L. McCarthy, Phys. Rev. **131**, 2133 (1963).

[11]J. Kleinfelder *et al.*, Nucl. Phys. **A370**, 205 (1981).

[12]S. Gales *et al.*, Phys. Rev. Lett. **48**, 1593 (1982); S. Gales *et al.*, Phys. Rev. C **31**, 94 (1985).

[13]T. Tamura, Phys. Rep. **14**, 59 (1974).

[14]C. M. Perey and F. G. Perey, At. Data Nucl. Data Tables **17**, 1 (1976).

[15]S. Chen *et al.*, Nucl. Phys. **A197**, 97 (1972).

[16]T. R. Anfinsen *et al.*, Nucl. Phys. **A157**, 56 (1970).

[17]G. A. Hutlin, S. Sen, W. A. Yoh, and A. A. Rollefson, Nucl. Phys. **A227**, 389 (1974).

[18]W. R. Coker, Phys. Rev. C **7**, 2426 (1973); W. R. Coker and G. W. Hoffmann, Z. Phys. **263**, 179 (1973).

[19]B. T. Kim, T. Udagawa, and T. Tamura, Phys. Rev. C **33**, 1270 (1986).